Journal of Power Sources 215 (2012) 248–257

Contents lists available at SciVerse ScienceDirect

Journal of Power Sources

journal homepage: www.elsevier.com/locate/jpowsour

Development of a lifetime prediction model for lithium-ion batteries based on extended accelerated aging test data

Madeleine Ecker*, Jochen B. Gerschler, Jan Vogel, Stefan Käbitz, Friedrich Hust, Philipp Dechent, Dirk Uwe Sauer

Institute for Power Electronics and Electrical Drives (ISEA), RWTH Aachen University, Jaegerstrasse 17-19, D-52066 Aachen, Germany

HIGHLIGHTS

- Extended accelerated aging tests on lithium-ion batteries.
- Semi-empirical aging model based on extended calendar aging data.
- Impedance-based electro-thermal model coupled to aging model.
- Lifetime prediction under real application condition possible concerning capacity fade.

ARTICLE INFO

Article history:
Received 28 February 2012
Received in revised form
27 April 2012
Accepted 6 May 2012
Available online 12 May 2012

Keywords:
Lithium-ion
Aging
Lifetime prognosis
Battery model
HEV

ABSTRACT

Battery lifetime prognosis is a key requirement for successful market introduction of electric and hybrid vehicles. This work aims at the development of a lifetime prediction approach based on an aging model for lithium-ion batteries. A multivariable analysis of a detailed series of accelerated lifetime experiments representing typical operating conditions in hybrid electric vehicle is presented. The impact of temperature and state of charge on impedance rise and capacity loss is quantified. The investigations are based on a high-power NMC/graphite lithium-ion battery with good cycle lifetime. The resulting mathematical functions are physically motivated by the occurring aging effects and are used for the parameterization of a semi-empirical aging model. An impedance-based electric-thermal model is coupled to the aging model to simulate the dynamic interaction between aging of the battery and the thermal as well as electric behavior. Based on these models different drive cycles and management strategies can be analyzed with regard to their impact on lifetime. It is an important tool for vehicle designers and for the implementation of business models. A key contribution of the paper is the parameterization of the aging model by experimental data, while aging simulation in the literature usually lacks a robust empirical foundation.

1. Introduction

Lifetime prediction for lithium-ion batteries under real operation conditions is a key issue for a reliable integration of the battery not only into the vehicle but also for stationary applications and for warranty issues. As aging tests using real operation conditions are very time and cost intensive, accelerated aging tests are discussed to be a powerful method. To extrapolate data obtained from accelerated aging test to real life conditions, aging models are required. So far simple model approaches for lifetime predictions have been reported in literature, like e.g. approaches based on neuronal networks [1]. These approaches usually lack the ability to make extrapolations to conditions that were not used in the learning test set. On the other hand, physic-chemical models have been developed, focusing on the description of single aging mechanisms like formation of solid electrolyte interphase (SEI) [2,3], mechanical stresses [4], etc. These models have been used for parameter studies, helpful to understand the ongoing process. Nevertheless they are not appropriate for fast lifetime predictions, as they are difficult to parameterize and only describe single mechanisms. This work aims at a compromise between physico-chemical and simple neuronal network model approaches. A physical approach based on an impedance model, able to extrapolate the data from accelerated aging tests to get real life condition lifetime predictions is presented here. It is an important goal of this semi-empirical approach to derive a set of equations for describing

* Corresponding author. Tel.: +49 241 8096977; fax: +49 241 8092203.
E-mail address: er@isea.rwth-aachen.de (M. Ecker).

0378-7753/$ – see front matter © 2012 Elsevier B.V. All rights reserved.
doi:10.1016/j.jpowsour.2012.05.012

the aging using mathematical expressions that are close to the main degradation mechanisms.

Aging in lithium-ion batteries leads to increase of inner resistance, capacity and power loss as well as to changes in impedance spectra due to electrochemical and mechanical processes. Aging strongly depends on temperature, SOC or rather electrode potential, cycling depth and charge throughput [5–7]. Few studies are reported in literature, investigating the calendar and cycle life of different cells using large test matrixes [7–10]. These studies illuminate the aging characteristics of lithium-ion batteries. But so far, this knowledge has not been utilized to develop an aging model that is able to predict the lifetime cycle of real application. Wang et al. [10] made the attempt of a lifetime prediction model based on cycle aging results, but didn't include the strong influence of SOC on aging.

Aging models based on mathematical functions obtained from extended aging tests can be directly linked to impedance-based models, which determine electrical and thermal behavior of the battery [11,12]. Coupling of impedance-based thermo-electrical battery models with aging models enables investigation of the dynamical interaction between thermal, electrical and aging behavior of the battery. A higher temperature for example causes a faster aging and therefore a faster increase in the inner resistance, affecting the electrical performance of the battery. These relations have been investigated in [13] but lacking a profound parameterization of the developed model using aging test results. This work will focus on the parameterization of the aging model by experimental data using extended aging test results.

2. Experimental

To parameterize impedance-based aging models, extensive aging tests are necessary. In this work a lithium-ion high power pouch cell with a nominal capacity of 6 Ah and a nominal voltage of 3.6 V was used. The anode consists of hard carbon, the cathode of $LiNi_{1/3}Mn_{1/3}Co_{1/3}O_2$ (NMC) as active material. Cells with similar characteristics are typically used in hybrid electric vehicle (HEV) applications.

Extended accelerated calendar aging tests have been performed by storing batteries at constant voltage at different temperatures and different SOC. The test matrix is shown in Table 1. Three cells have been tested under the same condition in order to get relevance statistic. At regular intervals of 6 weeks capacity tests, measurements of the inner resistance of the battery and electrochemical impedance spectroscopy (EIS) were performed. Some cells were stored at float conditions (constant voltage), whereas for other cells storage conditions were applied (open circuit). The cells stored with open circuits showed self-discharge processes over time. Therefore, the average voltage during the 6 weeks of storage is used for evaluation of the data. In general, aging tests performed at float conditions are more desirable for the parameterization of aging models, as they ensure constant conditions.

The capacity was determined by a 1C discharge following a standard charge of the cell. For calculation of the inner resistance a high pulse power characterization profile as defined e.g. by VDA (German association of the automotive industry) [14] at different depths of discharge was used. Therefore a 18s 4 C-rate discharge pulse followed by a 40 s rest period and a 10 s 3 C-rate charge pulse also followed by a 40 s rest period was employed. The voltage response to this pulse at 20% DOD is shown in Fig. 1. In this work the so called overall discharge resistance at 20% DOD is used for the aging analysis. The overall discharge resistance is calculated by the difference between peak voltage U_1 after the 18 s discharge and the voltage U_2 after the 40 s rest period, divided by the discharge current ($R_{DCH} = (U_1 - U_2)/I_{DCH}$). For the battery considered in this work, the evolution of resistance over lifetime is nearly identical for different resistance definitions. Therefore the overall discharge resistance can be considered as representative for all resistances.

Impedance spectra were measured at different DOD (0%, 20%, 50%, 80%) in galvanostatic mode using frequency range from 5 kHz to 10 mHz. All spectra were measured without superposed DC current at 23 °C. For the measurement the laboratory instrumentation, the so called ISEA EISmeter [15], developed at ISEA several years ago was used. The EISmeter is still being further improved and is needed for high-precision impedance measurements on batteries.

Additionally cycle life tests were performed using a realistic current profile for HEV according to VDA (see Fig. 2). The current rates have been adjusted according to the manufactures cell specifications, namely a maximum continuous charge current of 5 C and 20 C for a 5 s pulse. The batteries were cycled at approx. 40 °C with a cycle depth of 20% around three different mean SOC. The cells were cycled between 60% and 80%, 45%–65% and 30%–50% SOC. The temperature was adjusted via a temperature sensor during cycling in order to ensure a cell temperature of 40 °C.

Table 1
Test matrix of calendar aging tests performed on 6Ah high power lithium-ion batteries with NMC as cathode material.

T / SOC	20 % (3,05 V)	50% (3,51 V)	80 % (3,92 V)	100 % (4,10 V)
25 °C			X	
35 °C	X	X		X
50 °C	X	X	X	X
65 °C		X		X

3. Calendar and cycle aging results

In order to develop and parameterize an aging model, the calendar aging tests were evaluated. In this section the most important results of the aging data are discussed and summarized to support the assumptions made for the setup of the model.

It is widely known from literature, that electrolyte decomposition and the corresponding formation of solid electrolyte interphase (SEI), is the dominant aging process in most graphite-based lithium-ion batteries during storage leading to capacity decline (due to loss of active lithium) and impedance rise (due to increase in film layer thickness) [7,16–18]. Theoretical derivations of the

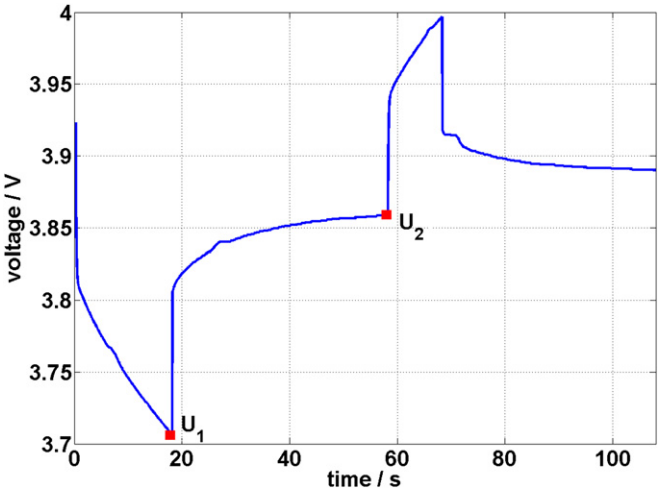

Fig. 1. Voltage response of the cell to the high pulse power characterization profile (VDA) at 20% DOD and 23 °C.

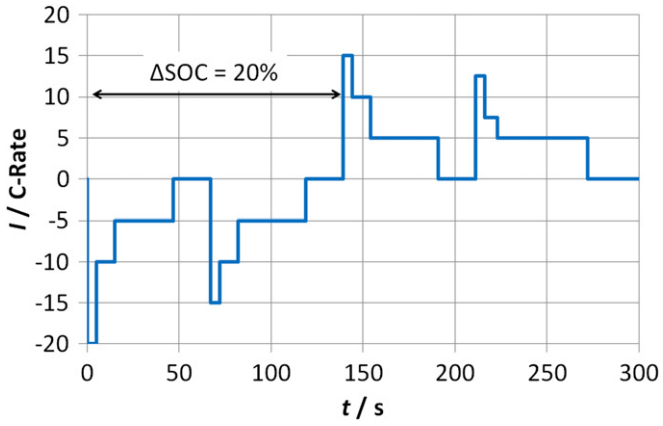

Fig. 2. HEV profile applied to the batteries.

time dependency of the SEI growth rate are quite opposing. Broussely et al. [7] for example describe a SEI formation process that takes place at the SEI/electrolyte interface, leading to the conclusion, that the electronic conductivity of SEI is the rate limiting step of formation. Ploehn et al. [16] in contrast state a SEI formation that takes place at the anode/SEI interface and is limited by solvent diffusion process. Nevertheless all theories lead to the conclusion that the formation process evolves with a square root of time dependency. A similar trend can be found in the aging behavior of capacity loss and internal resistance growth characteristics measured in this work for different storage conditions. Fig. 3a shows the actual capacity and Fig. 3b the inner discharge resistance over time for cells stored at 50% SOC at different temperatures. In section 4 it will be shown, that the square root of time dependency indeed gives the best fitting result in comparison to various other fitting functions describing the time evolution of the experimental aging data. The spike in the resistance and capacitance after 30 weeks (Fig. 3) is due to a measurement error, where the cells were not well connected.

Fig. 4 shows the influence of storage voltage (Fig. 4a) and storage temperature (Fig. 4b) on aging. The logarithm of capacity fade to basis 2 is plotted over voltage and over invers of temperature, respectively. This logarithmic scale is used, because rule of thumb postulates for lithium-ion batteries an aging rate that doubles, as temperature increases by 10 °C. In both graphs linear tendencies can be observed. Therefore it is assumed in the following, that capacity fade depends on voltage and temperature in an exponential way. Deviations from exponential behavior have been accepted in favor for physically motivated finctions. Similar aging behavior was observed regarding the internal resistance of the cell.

Concerning temperature, this result is in good accordance with Arrhenius law, describing the exponential dependency of reaction rate on temperature. As aging effects during storage are only due to parasitic side reactions, Arrhenius law can be applied here. Therefore, most battery technologies reveal an exponential temperature behavior and usually 3 or 4 different temperature points in the test matrix are sufficient to parameterize an aging model. To obtain nice Arrhenius behavior, storage temperatures below 60 °C are desirable. It has to be mentioned here, that for the storage temperature of 65 °C used in this tests chemical reactions are supposed to occur, that are not expected at lower temperatures. This leads to deviations from exponential behavior in Fig. 4b. Some of the cells stored at 65 °C even showed gassing processes, leading to a fast death of cell. These cells were not considered in the following.

The voltage dependency in contrast can be quite different, depending on the electrode material used in the cell and the corresponding phase transitions, during intercalation. Depending on

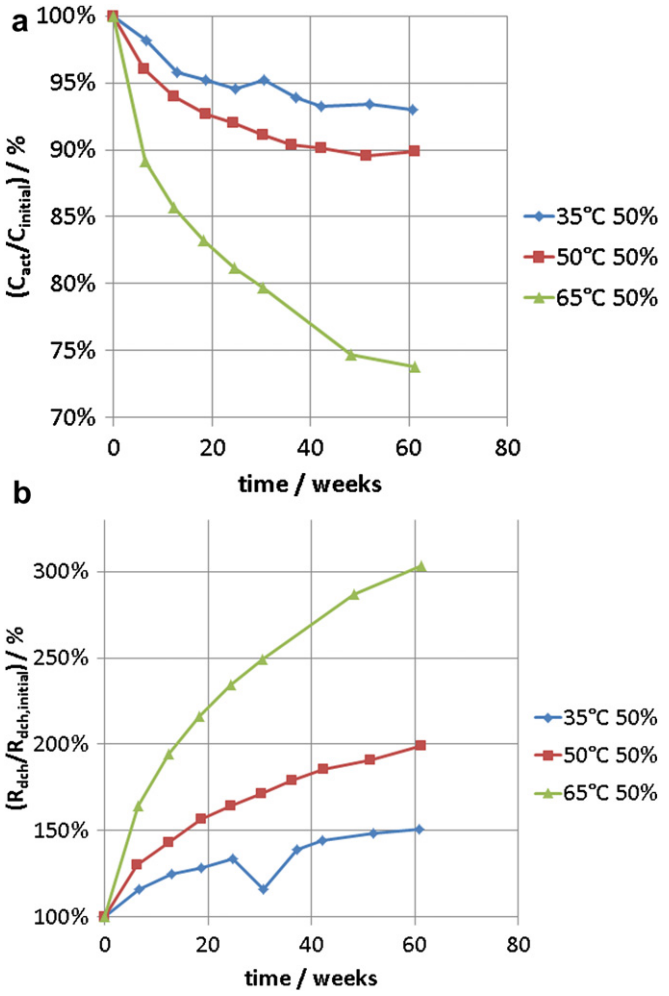

Fig. 3. Capacity normalized to initial value (a) and inner resistance normalized to initial value (b) over time is shown for cells stored at 50% SOC at different temperatures. Mean values of three cells stored at the same conditions are displayed.

the existing phases and phase changes during cycling, the material can show various aging behavior. In some cases of NMC based batteries even a minimum of aging rate could be measured e.g. at SOC around 80% during storage. In $LiMn_2O_4$ Materials Mn dissolution can lead to an increase in aging at lower SOC [19]. Also the electrolyte and additives account for the voltage range where electrolyte decomposition is favored. Therefore, depending on the cell considered, more detailed investigation of the impact of voltage can be necessary in order to understand its influence.

Similar to capacity fade and resistance increase, the obtained impedance spectra were evaluated according to aging dependencies on storage time, temperature and voltage. Fig. 5a shows the evolution of full-cell impedance spectra during aging for a cell stored at 65 °C and 50% SOC. It can be seen, that especially the intercept with the real axis, usually related to ohmic resistances like resistance of current collector and electrolyte, is increasing with proceeding aging. Additionally the mid-frequency semi-circle is enlarging, accounting for the increase of SEI resistance, charge transfer resistance and changes in the behavior of double layer capacity. It was assumed here, that the anode SEI contributes to this semi-circle of the full-cell impedance-spectrum according to [20]. The aging behavior shown here is specific to the cell considered. Depending on the cell behavior can change a lot. To evaluate these tendencies in detail, an electric circuit network, shown in Fig. 5b, consisting of an

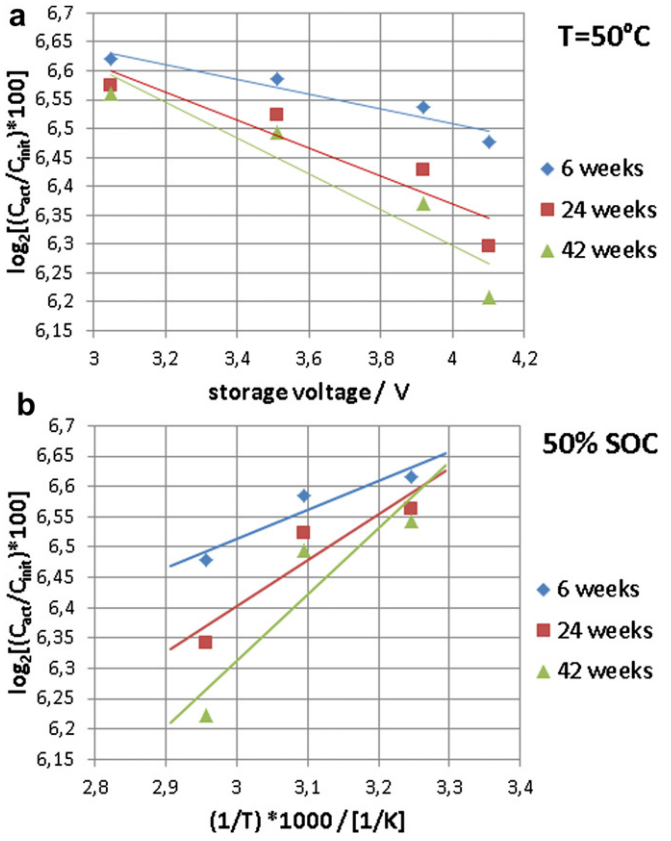

Fig. 4. a) Normalized capacity fade in a logarithmic scaling to basis 2 over storage voltage for different state of health. The cells were stored at 50 °C. b) normalized capacity fade in a logarithmic scaling to basis 2 over the invers temperature for different state of health. The cells were stored at 50% SOC. The mean values of the cells tested are shown here.

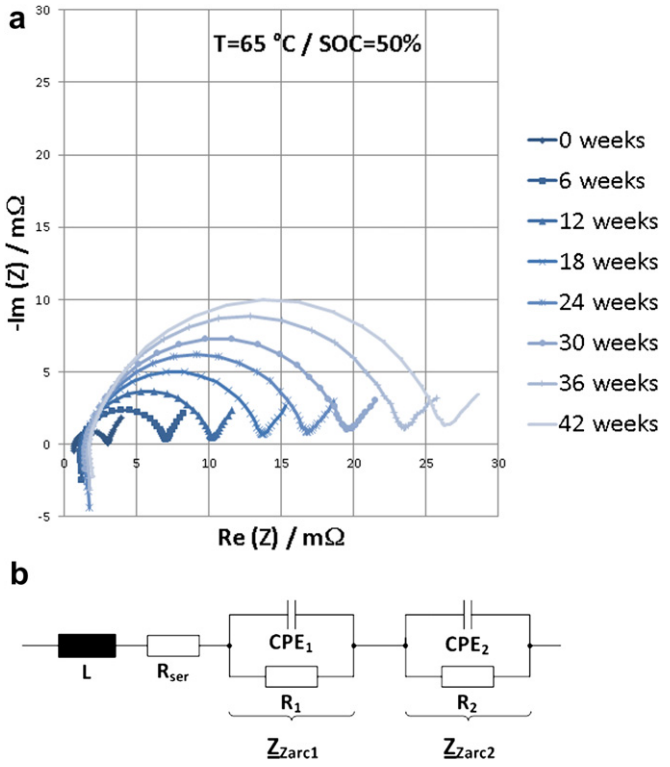

Fig. 5. a) Impedance spectra of a cell stored at 65 °C and 50% SOC at different state of health. The impedance spectra were measured at 23 °C and 80% SOC. b) electric circuit network that was used to evaluate the impedance spectra.

inductance, a serial resistance and two ZARC-elements, was used to describe the impedance spectra. The ZARC-element consists of a resistance and a constant phase element in parallel, described by the parameters R, A and φ [21,22]:

$$\underline{Z}_{ZARC} = \frac{R}{1 + R\,A(j\omega)^{\Phi}},\ \Phi \in [0,1] \tag{1}$$

The inductance describes the inductive part of the spectra, the serial resistance the intercept with the real axis, the first ZARC-element accounts for the mid-frequency semi-circle and the second ZARC-element was used to describe the diffusion behavior. Following [23] the Warburg impedance can be replaced by a ZARC-element and a constant phase element in series.

Fig. 6a shows the time evolution of the impedance parameters R_{ser}, R_1 and A_1. The sensitivity of the impedance parameters L, φ_1 and the parameters of the second ZARC-element on aging is small and the data reveal a large scattering over time. Therefore no further investigation has been conducted. The parameter R_1 increases faster in comparison to R_{ser} leading to the supposition, that SEI formation is the dominant aging process in the cell. Similar to the large signal measurement results, the impedance parameter show a square root of time dependency over lifecycle. Also the temperature and voltage impact the aging of impedance parameters in an exponential way, as expected from the theory of SEI formation. The only deviation from exponential behavior was found for the voltage dependency of the impedance parameter R_{ser}.

Fig. 6b shows a more parabolic relation between R_{ser} and voltage, which can be related to corrosion of current collector and degradation of electrolyte, increasing the ohmic resistance at low SOC. This is in contrast to the tendencies of capacity fade that decreases with lower SOC. Therefore a parabolic function is used to fit the voltage dependency of R_{ser} to the aging data in the following.

Fig. 7 shows the evolution of the OCV curve over aging for cells stored at 50 °C and 50% SOC. In Fig. 7a the OCV over DOD normalized to nominal capacity and in Fig. 7b the OCV over DOD normalized to actual capacity is shown. Using the DOD normalized to nominal capacity, the OCV curve changes over aging. Using the DOD normalized to actual capacity in contrast, the OCV curve stays the same. The same findings hold for the other points in the test matrix as well. For the use in an aging model, this means, that it is not necessary to change the OCV curve according to the state of health of the battery, but to simply use the latter definition of DOD in order to adjust the OCV.

To compare calendar and cycle lifetime, Fig. 8 shows capacity and resistance over time for cells stored under different conditions and cells cycled with the current profile for HEV according to VDA (see Fig. 2) in different SOC ranges. It cannot be concluded from Fig. 8a, whether storage or usage of the battery leads to faster fade of capacity. For example, the cell stored at 35 °C and 50% SOC shows smaller capacity fade than the cell cycled at 40 °C between 45 and 65% SOC, as expected due to the difference in temperature. The same cell ages faster than the one cycled between 30 and 50% SOC at 40 °C, due to the higher SOC. Nevertheless, it can be seen, that the calendaric contribution to aging is the most pronounced. The results for the inner resistance (Fig. 8b) in contrast yield the surprising implication, that storage conditions have a stronger impact on impedance rise than cycling the battery. It can be seen in the figure, that a battery stored at 50% SOC and 35 °C has a faster degradation concerning impedance, compared to a battery cycled under even worse conditions, namely 40 °C and a mean SOC of 70%. This means, cycling the battery enhances the resistive life.

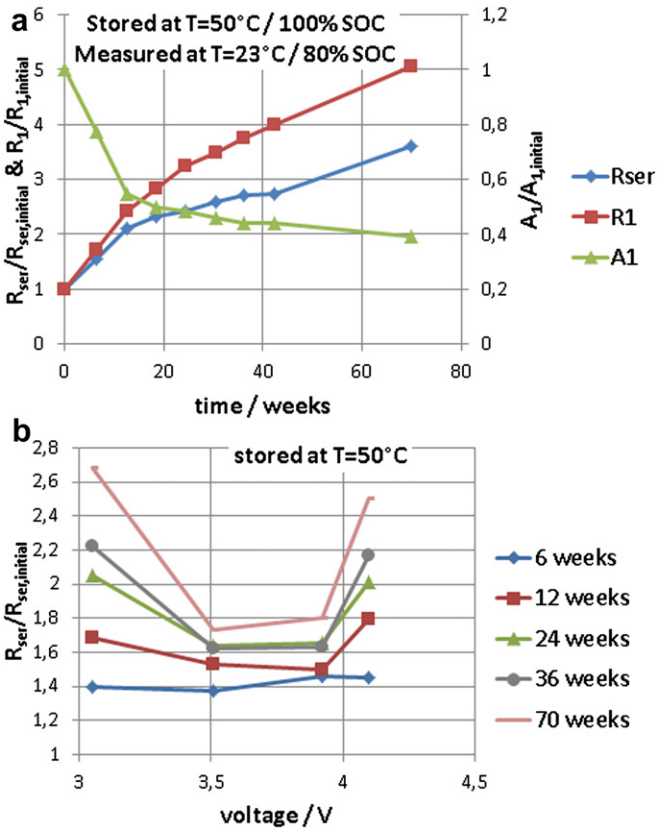

Fig. 6. a) Impedance parameters R_{ser}, R_1 and A_1 normalized to initial values over time for cells stored at 50 °C and 100% SOC. b) R_{ser} normalized to initial value over storage voltage for different states of health. The impedance spectra were measured at 23 °C and 80% SOC.

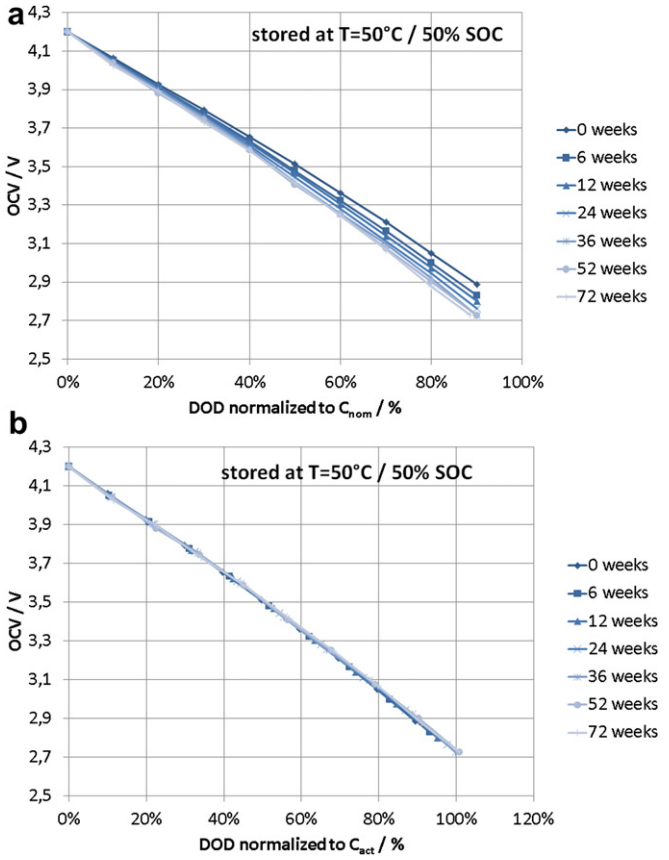

Fig. 7. OCV curves over aging for cells stored at 50 °C and 50% SOC are shown at different states of health. a) shows the OCV over DOD normalized to nominal capacity and b) The OCV over DOD normalized to actual capacity.

By linear extrapolation of the test results for cells cycled between 60% and 80% SOC, considering an end-of-life criterion of $C_{act} = 70\%\ C_{BOL}$, it can be shown that 30 000 equivalent full cycles can be obtained until the end of capacity life is reached. This cycle lifetime of the battery exceeds by far the requirements of application in HEVs. As for the application of lithium-ion batteries in HEVs, calendar life is the critical aspect of aging, only calendar aging test results will be considered in the following. The comparison of the evolution of inner resistance (Fig. 8b) between calendar and cycle aging shows, that a model based on calendar aging results only, can even be used for a worst case investigation concerning resistance.

4. Mathematical description of aging behavior

Based on the considerations of the previous section, a lifetime model following a semi-empirical approach can be developed. It has been shown from the aging tests, that the following simplifications and assumptions can be used:

- As the cycle life of the batteries exceeds by far the requirements of application, cycle aging is neglected in the following.
- Different definitions of resistances have been evaluated over aging. It has been found that they evolve in a similar way over aging. Exemplarily, the total discharge resistance was chosen for the parameterization of the aging model.
- The calendar aging of the cells evolves with a square root of time dependency. This assumption is also confirmed by the fitting results in the following discussion where various fitting functions are used to describe the time evolution of the experimental aging data (see Table 2).
- The rate of calendar degradation accelerates exponentially with temperature and voltage. Only for the voltage dependency of R_{ser} a parabolic function on voltage is used to fit the aging data.
- The aging behavior of the OCV curve can be accounted for, using the actual instead the nominal capacity for the definition of DOD.
- As the sensitivity of the impedance parameters L, R_2, A_2, φ_1 and φ_2 on aging is small and the data reveal no significant correlation over time, they are taken to be constant over time.

Based on these assumptions the following equations can be derived to fit the measured calendaric aging data:

$$L_{cal}(t,T,V) = L_{cal}(t_0,T,V)\cdot[1 + B(T,V)\cdot F(t)] \quad (2)$$

where L_{cal} is used for the evolution of capacity, inner resistance or impedance parameters either. $F(t)$ describes the time dependency and is related to the dominant aging processes or their combination:

$$F(t) = c_a \cdot t^{\beta} \quad (3)$$

c_a is a coefficient describing the rate of aging at reference conditions T_0 and V_0 depending on the specific process. Under the assumption of SEI formation being the dominant aging process, β becomes 0.5 [6].

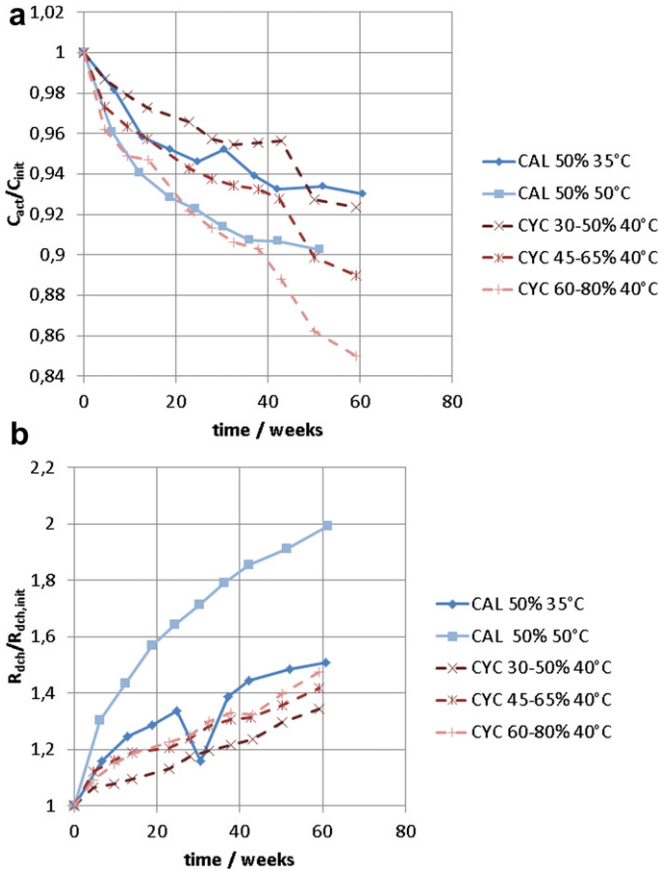

Fig. 8. Comparison of capacity fade (a) and resistance increase (b) over time between calendar and cycle aging. Test results of cells stored at different SOC and temperature levels are compared to cells cycled in different SOC ranges at 40 °C using the current profile for HEV according to VDA (see Fig. 2).

$B(T,V)$ describes the impact of temperature and potential on the calendar degradation rate according to:

$$B(T,V) = c_T^{\frac{T-T_0}{\Delta T}} \cdot c_V^{\frac{V-V_0}{\Delta V}} \tag{4}$$

The first factor describes the temperature impact on the aging rate, the second one the impact of the potential. c_T and c_V are fitting parameters, describing the impact of temperature and voltage on aging, respectively. T_0 and V_0 are reference temperature and voltage and can be chosen arbitrarily. For the following we chose $T_0 = 25$ °C and $V_0 = 3.5$ V. ΔT was set to 10 °C, meaning, that an increase in temperature by 10 °C results in an increase in aging by a factor c_T compared to reference conditions T_0. Similarly ΔV was set to 0.1 V. Similar equations have been also used by Bohlen et al. [11,12] to describe the aging behavior of super capacitors.

The only exception has been found in the aging behavior of the impedance parameter R_{ser}, where a parabolic dependency on voltage has been detected (see Fig. 6b). Therefore to describe the evolution of R_{ser} eq. (4) was substituted by:

$$B(T,V) = c_T^{\frac{T-T_0}{\Delta T}} \cdot \left(c_V \cdot \left(\frac{V-V_0}{\Delta V} \right)^2 + 1 \right) \tag{5}$$

Eq. (2) was used to fit the aging data presented in section 3, leaving the parameters c_a, c_T and c_V free for regression analysis. Non-linear least square algorithm was used for regression. The fits include data of the test matrix, introduced in section 2, containing about 30 batteries stored at different temperatures and voltages. For comparison, beside square root of time dependencies, as derived in eq. (2), also combinations of square root of time and linear time dependencies as well as combinations of square root of time and logarithmic time dependencies have been investigated in fittings. To assess the quality of fit an analysis of correlation coefficient R^2 was carried out. Table 2 compares the fit results of the different approaches for the capacity fade. Especially considering the linear behavior, it can be seen, that the linear contribution to the fit is very small or even zero. Therefore apart from increasing the number of free parameters the linear term did not yield

Table 2
Fit results for different mathematical functionalities for the capacity fade are shown.

Equation	Parameter	Parameter value	R^2	Number of free parameter
$\frac{C(t)}{C_{init}} = 1 + c_a \cdot c_V^{\frac{V-V_0}{\Delta V}} \cdot c_T^{\frac{T-T_0}{\Delta T}} \cdot \sqrt{t}$	c_a	−0.0064	0.9341	3
	c_V	1,.1484		
	c_T	1.5479		
$\frac{C(t)}{C_{init}} = 1 + c_V^{\frac{V-V_0}{\Delta V}} \cdot c_T^{\frac{T-T_0}{\Delta T}} \left[c_{a1} \cdot \sqrt{t} + c_{a2} \cdot t \right]$	c_{a1}	−0.0064	0.9341	4
	c_{a2}	0		
	c_V	1.1484		
	c_T	1.5479		
$\frac{C(t)}{C_{init}} = 1 + c_{a1} \cdot c_{V1}^{\frac{V-V_0}{\Delta V}} \cdot c_{T1}^{\frac{T-T_0}{\Delta T}} \cdot \sqrt{t} + c_{a2} \cdot c_{V2}^{\frac{V-V_0}{\Delta V}} \cdot c_{T2}^{\frac{T-T_0}{\Delta T}} \cdot t$	c_{a1}	−0.0053	0.9447	6
	c_{V1}	1.1392		
	c_{T1}	1.6389		
	c_{a2}	−0.00005		
	c_{V2}	1.87333		
	c_{T2}	0.59485		
$\frac{C(t)}{C_{init}} = 1 + c_a \cdot c_V^{\frac{V-V_0}{\Delta V}} \cdot c_T^{\frac{T-T_0}{\Delta T}} \cdot \log t$	c_a	−0.010392	0.9365	3
	c_V	1.15069		
	c_T	1.554253		
$\frac{C(t)}{C_{init}} = 1 + c_V^{\frac{V-V_0}{\Delta V}} \cdot c_T^{\frac{T-T_0}{\Delta T}} \left[c_{a1} \cdot \sqrt{t} + c_{a2} \cdot \log t \right]$	c_{a1}	−0.00291	0.9433	4
	c_{a2}	−0.00565		
	c_V	1.14959		
	c_T	1.55187		
$\frac{C(t)}{C_{init}} = 1 + c_{a1} \cdot c_{V1}^{\frac{V-V_0}{\Delta V}} \cdot c_{T1}^{\frac{T-T_0}{\Delta T}} \cdot \sqrt{t} + c_{a2} \cdot c_{V2}^{\frac{V-V_0}{\Delta V}} \cdot c_{T2}^{\frac{T-T_0}{\Delta T}} \cdot \log t$	c_{a1}	−0,00094	0.9604	6
	c_{V1}	1.055624		
	c_{T1}	2.255951		
	c_{a2}	−0.008921		
	c_{V2}	1.225323		
	c_{T2}	1.284523		

significant improvement compared to eq. (2). The fitting results for the expressions including a logarithmic term show, that also logarithmic time dependency can be an approach to describe calendar aging. The difference to the square root dependency is that the logarithmic time dependency is steeper in the beginning and gets flatter later. Therefore it overestimates the aging at the beginning, but yields better results after some time. As the logarithmic behavior lacks a physical explanation, we will focus on the square root dependency in the following. Square root function on time can be directly derived from theoretical investigation of SEI formation. The physical process behind the mathematical expression is the critical issue to ensure the ability of the model for extrapolations. Therefore the square root function is chosen even though other expressions give slightly better regression results.

In Table 3 the values of the resulting fitting parameters for capacity fade, resistance increase and impedance parameters using eq. (2) and the corresponding correlation coefficients R^2 are shown. The parameters describing the capacity evolution indicate an acceleration of aging by a factor of $c_T = 1.55$ caused by a temperature increase of $\Delta T = 10\ ^\circ C$ compared to T_0. For potential dependency of the capacity, fitting reveals an acceleration factor of $c_V = 1.15$ for an increase of $\Delta V = 0.1$ V. This differs from the rule of thumb, predicting that aging rate doubles by increasing the temperature by 10 °C. The aging rate at reference conditions T_0 and U_0 becomes $c_a = -0.0064$. Similar results are received for the inner resistance and the impedance parameters R_{ser}, R_1, A_1, differing slightly as they are impacted by different aging effects. Thus this approach convinces due to its simplicity and its physical correspondent.

Fitting results for the evolution of capacity and overall resistance during storage at 50% SOC at different temperatures are shown exemplarily in Fig. 9. The fittings for these values yield good results, with an R^2 of 0.934 and 0.96, respectively. It has to be kept in mind that data of about 30 cells at a variety of storage conditions have been fitted using one set of parameters. This of course yields deviations of the fit from the data at certain conditions. Fig. 9 shows also that the three cells which have been tested under same conditions at any working point scatter significantly. Therefore, the fits will always show a relative low R^2 value. Nevertheless the overall fitting result is unquestionable and shows clearly the dependency on the different impact parameters.

Equation (2) also yields good results for the description of the impedance parameters. For R_{ser} a parabolic voltage dependency was taken into account. Even though the data concerning impedance parameters are scattering more compared to the capacity and resistance data, correlation coefficients between 0.79 and 0.89 could be obtained. The scattering in the data is due to the additional fitting step to determine impedance parameters using the electric circuit diagram in Fig. 5b. The fitting results for the evolution of the impedance parameters R_{ser}, R_1 and A_1 for cells stored at 50% SOC at different temperatures are shown in Fig. 10.

5. Development of lifetime model

The fitting results of the calendar aging data can be used to develop a model to predict lifetimes under different operation conditions by combining an impedance-based electro-thermal model with the mathematical expressions obtained from the test results. Such a semi-empirical model approach for lifetime predictions has the advantage of an easy parameterization based on accelerated calendar life tests and an acceptable computing time. Moreover the approach enables extrapolations to different operation conditions, e.g. to lower temperature, as the mathematical equations derived in section 4 are based on physical aging processes in the battery. This is an advantage of such a model approach in comparison to e.g. models using neuronal network approaches.

The electrical model used in this work is an impedance-based model, using the electric circuit diagram in Fig. 5b with an additional serial capacity C_d (intercalation capacitance [24]) to calculate the voltage response of the cell to a current pulse. The electrical network is parameterized by impedance spectra measured at different temperatures and voltages. The resulting impedance parameters are given to the model as lookup tables for different temperatures and voltages. To parameterize the current dependency of the impedance parameters, the current dependency of the

Table 3
Fitting parameters for capacity fade, resistance increase and impedance parameters R_{ser}, R_1 and A_1 using eq. (2) and the corresponding correlation coefficients R^2.

	c_a	c_V	c_T	R^2
Capacity	−0.0064	1.1484	1.5479	0.934
Resistance	0.0484	1.0670	1.5665	0.96
R_{ser}	0.0206	0.0471	1.7586	0. 85
R_1	0.0766	1.0618	2.1437	0.89
A_1	−0.0457	1.0258	1.2248	0.79

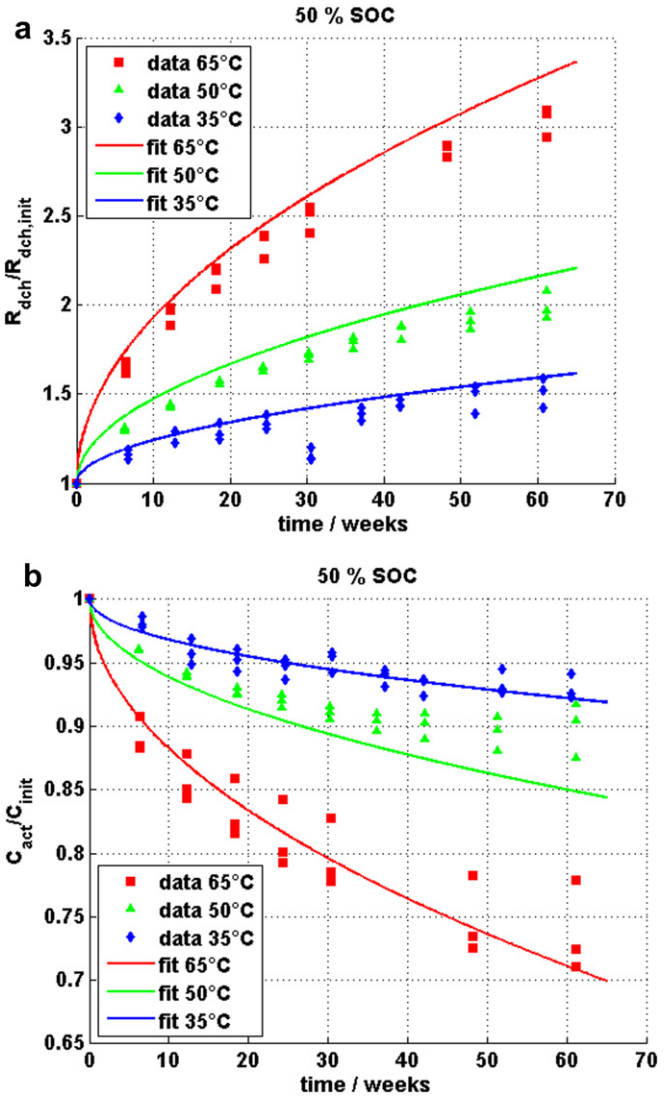

Fig. 9. Fitting results for a) Capacity fade (actual capacity normalized to initial capacity) and b) resistance increase (actual resistance normalized to initial resistance) over time using eq. (2) are shown for cells stored at 50% SOC at different temperatures. The dots mark the measured data results for the cells, the lines the fittings.

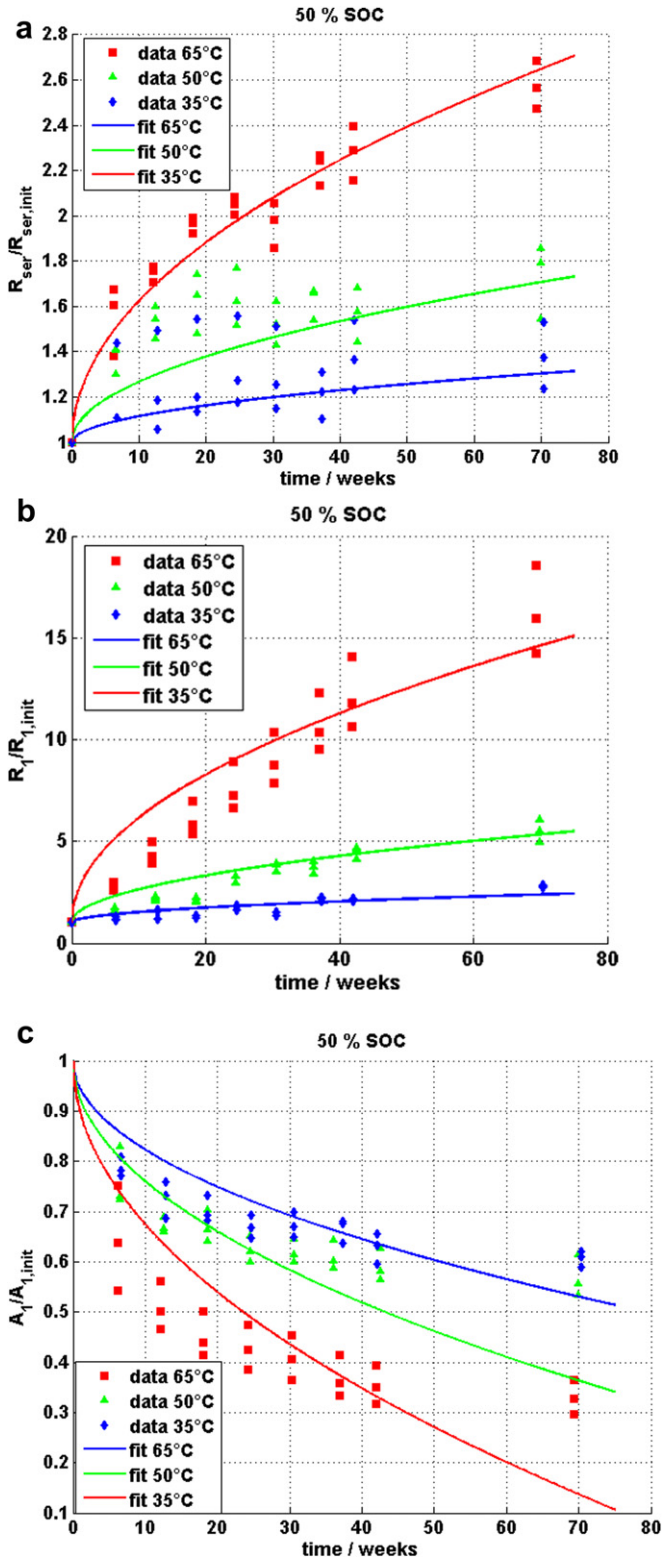

Fig. 10. Fitting results for the evolution of the impedance parameters a) R_{ser}, b) R_1 and c) A_1 using eq. (2) for cells stored at 50% SOC at different temperatures are shown. The values are normalized to the initial value. The dots mark the measured data results for the cells, the lines the fittings.

inner resistance obtained from high pulse power profiles was used. The thermal model is based on a simple thermal network including a joule heating as a one point source, a heat capacity and thermal conductivity in each direction in space to simulate heat transfer with the environment. More details on the thermo-electrical model can be found in [25], where also the validation of the model for the cell used in this work can be found. The thermal, as well as the dynamic electrical behavior can be simulated accurately. A similar approach was also used in [21,26].

As aging depends strongly on temperature and voltage, the lifetime model receives temperature and voltage calculated by the thermo-electrical model in each time step. The infinitesimal aging of the cell due to the predominating conditions, i.e. temperature and voltage, is calculated. Depending on the application and on the applied current profile, temperature and voltage vary over time. Therefore it is necessary to add up the incremental loss of lifetime in the model using equation (2):

$$L_{\mathrm{cal}}(t,T(t),V(t)) = L_{\mathrm{cal}}(t_0,T(t_0),V(t_0)) + \sum_{i=1}^{N} \frac{\mathrm{d}L_{\mathrm{cal}}(L_{\mathrm{cal}}(t_{i-1}),T(t_i),V(t_i))}{\mathrm{d}t_i}\Delta t_i \qquad (6)$$

In the semi-empirical aging model all parameters of the electrical model part, like capacity, inner resistance and impedance parameters are updated according to their actual state of health following equation (6) in each time step. It is important to note that we assumed the actual degradation, e.g. capacity fade and resistance to be dominated by SEI growth. As the rate of SEI growth is mainly determined by the layer thickness, capacity fade and resistance increase are directly proportional to change in layer thickness. Since not the ongoing time, but the layer thickness is the only continuous parameter during varying temperature and voltage, t has to be substituted by the actual capacity or resistance in equation (6), representing SEI thickness. Fig. 11 shows schematically the working principle of the model.

6. Simulation result

For the simulation a realistic current profile for HEV according to VDA was used to cycle the battery and to investigate the aging under realistic operation conditions. Using the profile shown in Fig. 2 the batteries were cycled at 40 °C between 60% and 80%, 45%–65% and 30%–50% SOC. The profile was also applied to cells

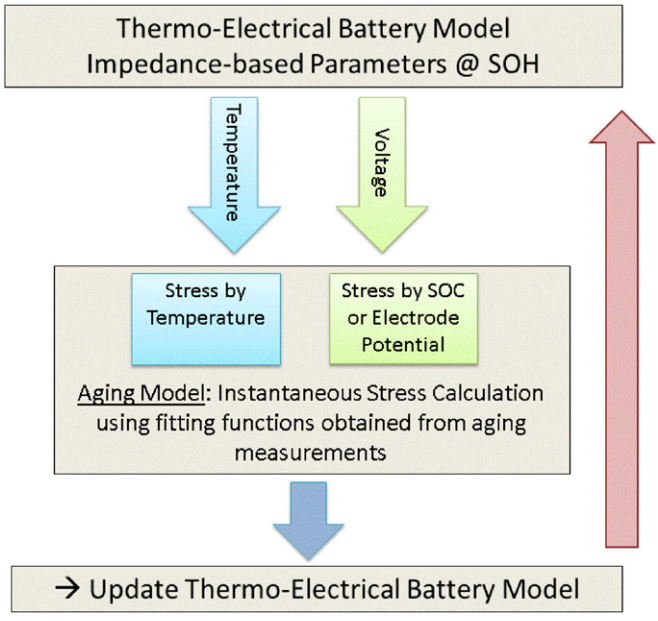

Fig. 11. Working principle of the semi-empirical aging model.

during aging tests as described in section 3. For the comparison with the cycle data from the test results no temperature model was used in the following simulation. The cell temperature was set to 40 °C over time, to make it comparable to the measurement where the cells were kept at 40 °C during cycling using temperature sensors.

Fig. 12 shows simulation results for capacity fade and resistance increase during cycling of the cells using the HEV profile. Wheras end of capacity life (80% of initial capacity) is already reached after about 2 years while cycling the battery between 60% and 80% SOC, even 6 years of lifetime can be obtained, when the battery is cycled only between 30% and 50% SOC. The higher state of charge leads to a faster degradation. It can also be seen, that the end of resistive life (initial resistance doubles) is reached much faster compared to end of capacity life.

Fig. 13 shows the comparison of the simulation with the measured data for verification of the model developed in this work. Capacity fade (Fig. 13a) reveals, that the lifetime model based on calendar aging results only, is indeed able to make predictions for lifetimes even under usage of the battery. The measured cycling data are reproduced by the simulation results quite well. Considering the resistance fade (Fig. 13b) it can be concluded, that the model underestimates the battery lifetime by far. This is in accordance with the results from section 3 as Fig. 8a shows clearly, that during storage the battery ages much faster than during cycling under similar conditions. Thus a model only based on calendar aging results overestimates the resistive aging of the battery investigated in this study. Therefore, it can be concluded that the model based on calendar aging results can only make reliable lifetime predictions concerning capacity fade. The results show that different aging effects occur during cycling in comparison to storage, influencing the resistance of the battery. It can be

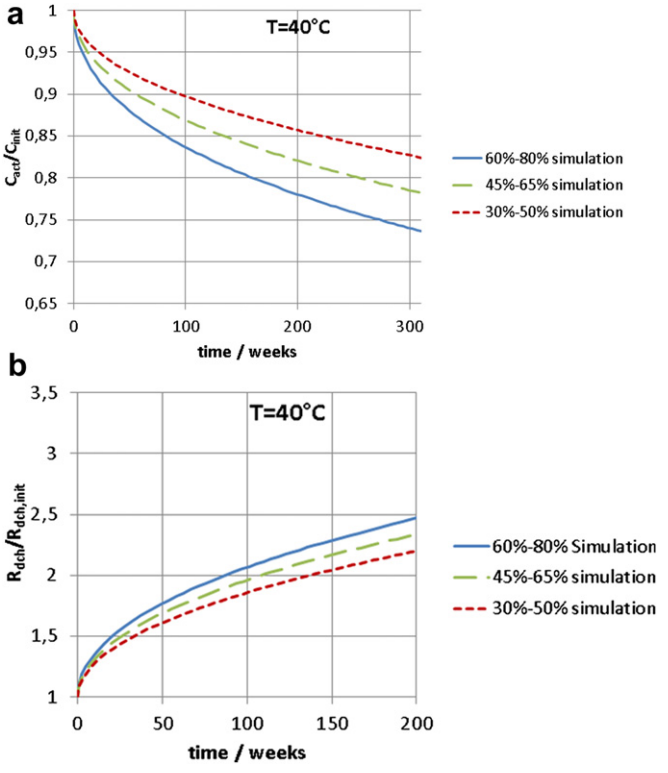

Fig. 12. Simulation results for a) capacity fade (actual capacity normalized to initial capacity) and b) resistance increase (actual resistance normalized to initial resistance) over time is shown. The cells are cycled at 40 °C with the HEV profile between different SOC.

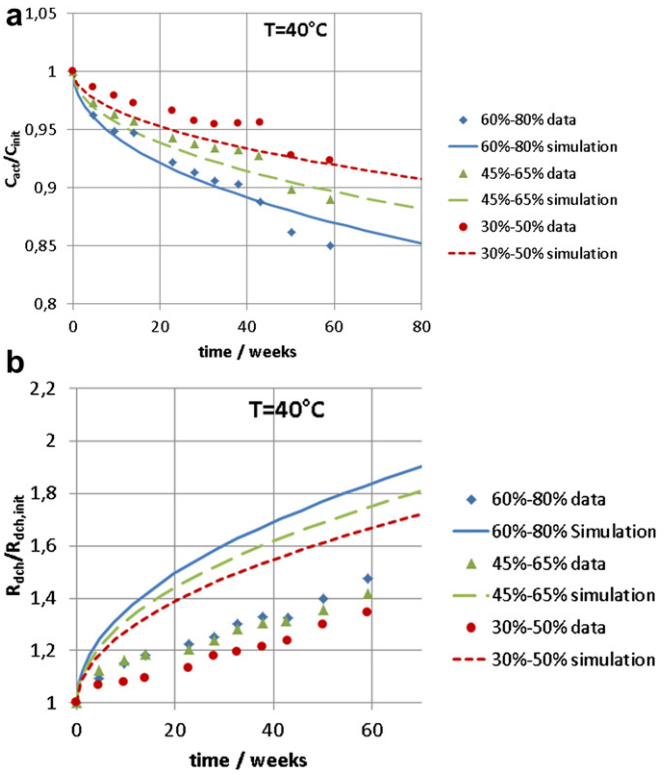

Fig. 13. Comparison between simulation and measurement for a) Capacity fade (actual capacity normalized to initial capacity) and b) resistance increase (actual resistance normalized to initial resistance) over time, for cells cycled at 40 °C with the HEV profile between different SOC.

speculated, that the structure of the SEI is different when formed during calendaric aging or during cycling. The overall lithium content of SEI and therefore the capacity loss seem to be quite independent from the way the battery is operated. But during storage a denser SEI layer is formed with lower conductivity for lithium ions. On the other hand, the low resistance increase during cycling can be also due to effects of mechanical stresses, leading to smaller particle sizes and therefore to bigger surface areas. In order to ameliorate lifetime predictions, the relation between calendar and cycle life has to be investigated in more detail by post-mortem analysis to account for this effect.

Fig. 14 shows a comparison between simulations, where the impedance parameters R_{ser}, R_1 and A_1 were updated according to the state of health of the battery, simulations where only R_{ser} and R_1 were updated and simulations where the adaptation of impedance parameters according to state of health was not considered at all. For the simulations the same current profile as before was used. The cell was cycled in an SOC range between 60 and 80%. Ambient temperature was set to 40 °C and the thermal model discussed in section 5 was used to calculate the cell temperature. The impedance parameters are used in the electro-thermal model, to reproduce the dynamic behavior of the battery. Therefore, updating the impedance parameters according to state of health leads to a spread in voltage range, as the overpotential changes over lifetime. Additionally, aging of the impedance parameters induces a temperature rise. Overpotential and temperature change are mainly due to the resistances in the electrical circuit diagram (Fig. 5b). Therefore, if only the evolution of A_1 over lifetime is neglected, this does not impact the overall aging characteristic of the cell. The blue continuous and the red dotted line are overlapping in Fig. 14. But neglecting the aging of all impedance parameters, temperature and voltage range do not change over

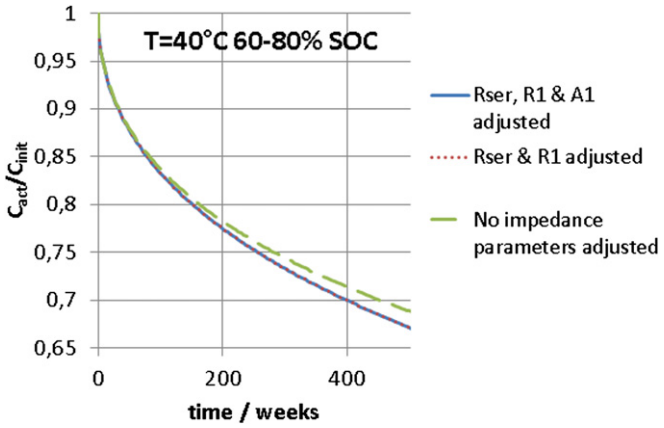

Fig. 14. Simulation of normalized capacity fade over time for cells cycled at 40 °C with the HEV profile between 60 and 80% SOC. The blue continuous line shows the result of a simulation, where the impedance parameters R_{ser}, R_1 and A_1 were updated according to the state of health of the battery, for the red, dotted line, only R_{ser} and R_1 were ajusted and the green dashed line displays results where the adaptation of impedance parameters according to state of health was neglected. (For interpretation of the references to colour in this figure legend, the reader is referred to the web version of this article.)

time, leading to an overestimation of lifetime. It can be seen in Fig. 14 that the impact of changing impedance parameters is quite small. The deviation in prediction of lifetime of a non-dynamic model in comparison to a dynamic model at 80% of initial capacity is about 9%. In a dynamic model the battery reaches 80% of initial capacity after 148 weeks, in a non-dynamic model after 161 weeks. Therefore, if a fast computation is necessary, or impedance parameters have not been measured over lifetime, neglecting their influence has only little impact on the result.

7. Conclusion

In this work a simulation model was presented to predict lifetime of a high power lithium-ion battery under realistic operation condition. The model approach couples an impedance-based electric-thermal model to a semi-empirical aging model, to account for the impact of aging on the dynamic behavior of the battery. The aging model is based on results obtained from extended accelerated aging tests, which were used to parameterize the model. From the results of the aging test, simplifications for the model approach could be derived. It was observed that calendar aging test results can be used for a first approximation of lifetime or even a worst case consideration, as cycle life of the batteries exceeds by far the requirements of application. Test results showed, that a square root of time dependency can be applied to the data, as well as an exponential behavior of aging on voltage and temperature. The aging behavior of the OCV curve was accounted for, using the actual instead of the nominal capacity for the definition of DOD. The sensitivity of the Impedance parameters L, R_2, A_2, φ_1 and φ_2 on aging is small and was therefore neglected. Mathematical functions, based on physical aging effects, were obtained from the test results to describe the aging behavior and to ensure the ability of the model to make extrapolations. The expressions were implemented in a semi-empirical aging model. Based on the model different drive cycles, use patterns and management strategies can be analyzed with regard to their impact on lifetime. Simulation results were compared to experimental data of cells that were cycled with a realistic HEV profile in different operation ranges. Concerning capacity fade, the model, based on calendar aging results, is able to make reliable lifetime predictions for a battery under operation. Considering inner resistance, the model overestimates the aging of the cell, as resistance increases much faster during storage, than under operation. In future work the relation between calendar and cycle life has to be investigated in more detail to account for this effect. The findings can be used to ameliorate the model approach. It has to be kept in mind that the findings presented here are only valid for the specific cell considered in this work. The results cannot be transferred to other cells even with the same chemistry.

Acknowledgment

This work has been done in the framework of the research initiative “KVN” funded by the German Federal Ministry for Education and Research, funding number 13N9973. Responsibility for the content of this publication lies with the authors.

References

[1] R. G Jungst, G. Nagasubramanian, H.L. Case, B.Y. Liaw, A. Urbina, T.L. Paez, D.H. Doughty, J. Power Sources 119–121 (2003) 870–873.
[2] P. Ramadass, Bala Haran, Parthasarathy M. Gomadam, Ralph White, Branko N. Popov, J. Electrochem. Soc. 151 (2004) A196–A293.
[3] J. Christensen, J. Newman, J. Electrochem. Soc. 151 (2004) A1977–A1988.
[4] J. Christensen, J. Newman, J. Solid State Electrochem. 10 (2006) 293–319.
[5] J. Vetter, P. Novák, R.M. Wagner, C. Veit, K.-C. Möller, J.O. Besenhard, M. Winter, M. Wohlfahrt-Mehrens, C. Vogler, A. Hammouche, J. Power Sources 147 (2005) 269–281.
[6] M. Broussely, S. Herreyre, P. Biensan, P. Kasztejna, K. Nechev, R.J. Staniewicz, J. Power Sources 97-98 (2001) 13–21.
[7] M. Broussely, P. Biensan, F. Bonhomme, P. Blanchard, S. Herreyre, K. Nechev, R.J. Staniewicz, J. Power Sources 146 (2005) 90–96.
[8] R.B. Wright, C.G. Motloch, J.R. Belt, J.P. Christophersen, C.D. Ho, R.A. Richardson, I. Bloom, S.A. Jones, V.S. Battaglia, G.L. Henriksen, T. Unkelhaeuser, D. Ingersoll, H.L. Case, S.A. Rogers, R.A. Sutula, J. Power Sources 110 (2002) 445–470.
[9] S.A. Bloom, E.G. Jones, V.S. Polzin, G.L. Battaglia, C.G. Henriksen, R.B. Motloch, R.G. Wright, H.L. Jungst, D.H. Case, J. Power Sources 111 (2002) 152–159.
[10] J. Wang, P. Liu, J. Hicks-Garner, E. Sherman, S. Soukiazian, M. Verbrugge, H. Tataria, J. Musser, P. Finamore, J. Power Sources 196 (2011) 3942–3948.
[11] O. Bohlen, J. Kowal, D.U. Sauer, J. Power Sources 172 (2007) 468–475.
[12] O. Bohlen, J. Kowal, D.U. Sauer, J. Power Sources 173 (2007) 626–632.
[13] J. B. Gerschler, H. Witzenhausen, F. Hust, D. U. Sauer, Three-Dimensional Performance and Lifetime Model for Lithium-Ion Batteries –Spatially-Resolved Models are Required for Accurate Simulation of Large-Sized Cells, Electric Vehicle Symposium (EVS-25) Shenzhen, China, Nov. 5-9, 2010.
[14] Test Specification for Li-Ion Battery Systems for Hybrid Electric Vehicles, Association of the German Automotive Industry (VDA), 2007, Release 1.0.
[15] E. Karden, Using low-frequency impedance spectroscopy for characterization, monitoring, and modeling of industrial batteries, Dissertation thesis, RWTH Aachen University, 2001, Shaker Verlag, ISBN 3-8265-9766-4.
[16] H.J. Ploehn, P. Ramadass, R.E. White, J. Electrochem. Soc. 151 (2004) A456.
[17] D. Aurbach, J. Power Sources 89 (2000) 206–218.
[18] R. Spotnitz, J. Power Sources 113 (2003) 72–80.
[19] Y. Nishi, J. Power Sources 100 (2001) 101–106.
[20] W. A. van Schalkwijk, B. Scrosati, Advances in lithium-ion batteries, ISSN: 9780306473562.
[21] S. Buller, M. Thele, K. Kahlen, R.W. De Doncker, IEEE Transactions Industry Applications 41 (3) (2005) 742–747.
[22] S. Buller, Impedance-based simulation models for energy storage devices in advanced automotive power systems, Dissertation, RWTH Aachen, Shaker Verlag, 2003, ISBN 3-8322-1225-6.
[23] Dirk Linzen, Impedance-Based Loss Calculation and Thermal Modeling of Electrochemical Energy Storage Devices for Design Considerations of Automotive Power Systems, Dissertation, RWTH Aachen, Shaker Verlag, 2006, ISBN: 978-3-8322-5706-4.
[24] D. Aurbach, B. Markovsky, M.D. Levi, E. Levi, A. Schechter, M. Moshkovich, Y. Cohen, J. Power Sources 81–82 (1999) 95–111.
[25] S. Käbitz, D. U. Sauer, Impedance spectroscopy to model lithium-ion batteries, International Workshop on Impedance Spectroscopy, October 2011, Chemnitz, Germany.
[26] D. Andre, M. Meiler, K. Steiner, H. Walz, T. Soczka-Guth, D.U. Sauer, J. Power Sources 196 (2011) 5349–5356.